

# Light-Actuated Anisotropic Microactuators from CNT/Hydrogel Nanocomposites

Aoife Gregg, Michael F. L. De Volder,\* and Jeremy J. Baumberg\*

Over the past decades, functional hydrogels that respond to a variety of mechanical and chemical stimuli with a volume change of more than 100% have been developed. Despite this impressive behavior, practical applications of conventional hydrogels are limited by the need to transform their isotropic swelling/contraction into useful deformations, as well as their slow response times. Here, these challenges are addressed by combining poly(*N*-isopropylacrylamide) (PNIPAM), a widely used temperature-responsive polymer, with carbon nanotubes (CNTs). To ensure strong PNIPAM–CNT cohesion, the hydrogel is synthesized directly on the CNT surfaces using *in situ* redox polymerization. The anisotropy of vertically-aligned CNT forests is used to transform the isotropic (de)swelling of PNIPAM into anisotropic motion. This material combination is particularly attractive because the high optical absorption and heat conductivity of carbon nanotubes converts light irradiation into PNIPAM actuation. A wide variety of CNT-skeleton microstructures are tested to reveal a range of actuation behaviors. The authors demonstrate fast reversible movement, active switching from low to high light absorption states, lattice shape changes, and good cycling stability.

exposure to stimuli such as temperature or pH. The size change arises from changes in solvation so that a hydrogel swells with water when the gel is hydrophilic and expels water when it is hydrophobic. Temperature-responsive volume-switchable hydrogels with a lower critical solution temperature (LCST) are hydrophilic below their critical solution temperature ( $T_c$ ) and hydrophobic above, thus shrinking when heated above  $T_c$ .

Poly(*N*-isopropylacrylamide) (PNIPAM) is a favored temperature-responsive volume-switchable hydrogel with an LCST of  $\approx 32$  °C. Its popularity derives from having an LCST just above room temperature and close to human body temperature, as well as the tunability of its LCST by introducing co-monomers, and the possibility to confer responsiveness to stimuli such as pH by modifying the monomer composition.<sup>[3,4]</sup> However, applications of conventional PNIPAM are limited by its

isotropic volume switching, slow response times, and the difficulty of achieving controllable pre-designed movement.<sup>[5,6]</sup> It is thus often modified to address these limitations. PNIPAM has been combined with materials such as graphene oxide,<sup>[7–12]</sup> iron oxide nanoparticles,<sup>[13–18]</sup> clay,<sup>[19]</sup> and carbon nanotubes<sup>[20,21]</sup> to add properties including electrical and thermal conductivity, and response to light and magnetic fields. Fabrication methods such as photopatterning,<sup>[13,22–25]</sup> electrospinning,<sup>[26]</sup> origami,<sup>[13,21,27,28]</sup> grafting to pre-fabricated nanopillars or nanosheets,<sup>[29–35]</sup> precipitation polymerization,<sup>[1,36,37]</sup> 3D-<sup>[38–40]</sup> and ion-inkjet<sup>[41]</sup> printing have been used to create nano- and microscale hydrogel actuators with more complex controlled motion and faster response times. However challenges remain, particularly in developing anisotropic motion.

In this paper, carbon nanotubes (CNTs) are used as both an additive to the PNIPAM and as a skeleton for fabricating hydrogels in a wide range of shapes and sizes. CNTs are well known for their remarkable strength, with Young's modulus up to 1 TPa and an inherent tensile strength of over 100 GPa.<sup>[42–44]</sup> They are highly durable and resistant to fatigue over millions of strain cycles.<sup>[43,45,46]</sup> CNTs are highly electrically and thermally conductive, and vertically-aligned forests of carbon nanotubes act as pseudo-blackbodies with up to 99% broadband absorption of light from UV to the far IR.<sup>[47,48]</sup> CNTs have previously been combined with PNIPAM and other hydrogels in a variety of ways.<sup>[49]</sup> Typically CNTs have been incorporated by either dispersing them in a polymer or pre-polymer solution,<sup>[21,50–54]</sup>

## 1. Introduction

Hydrogels are an ideal material for reversible shape-changing structures due to the flexibility in their fabrication techniques, their biocompatibility, low cost, scalability, and the wide range of possible constituent materials. They show many tunable features and capabilities, depending on the chemistry of the constituent polymers.<sup>[1,2]</sup> Hydrogels with a switchable volume are of particular interest: these change size dramatically upon

A. Gregg, J. J. Baumberg  
Cavendish Laboratory  
Department of Physics  
University of Cambridge  
J.J. Thomson Avenue, Cambridge CB3 0HE, UK  
E-mail: jjb12@cam.ac.uk

A. Gregg, M. F. L. De Volder  
Institute for Manufacturing  
Department of Engineering  
17 Charles Babbage Road, Cambridge CB3 0FS, UK  
E-mail: mfl2@cam.ac.uk

 The ORCID identification number(s) for the author(s) of this article can be found under <https://doi.org/10.1002/adom.202200180>.

© 2022 The Authors. Advanced Optical Materials published by Wiley-VCH GmbH. This is an open access article under the terms of the Creative Commons Attribution License, which permits use, distribution and reproduction in any medium, provided the original work is properly cited.

DOI: 10.1002/adom.202200180

or by functionalizing CNTs such that polymer growth and crosslinking are initiated directly on the nanotube.<sup>[55–61]</sup> The presence of CNTs has so far been used to improve hydrogel response times by enhancing mass transport of water via increased porosity of CNT/hydrogel composites,<sup>[21]</sup> add light responsivity<sup>[21,60,62–64]</sup> and electrical conductivity,<sup>[50,55,59,65,66]</sup> and improve mechanical properties.<sup>[50–52,54,56]</sup> A unique opportunity offered by CNTs that is under-explored in hydrogel composites is the ability to assemble aligned CNTs into 3D structures by using a combination of lithography and chemical vapor deposition of CNTs.<sup>[67,68]</sup>

In nature, isotropic swelling of a matrix is often combined with carefully architected fiber arrangements to transform isotropic swelling into complex movement, such as in pinecones and other seed dispersal units.<sup>[69,70]</sup> Aligned CNT structures have previously been proposed as a scaffold to transform the swelling of hygroscopic gels into a controlled motion to achieve, for instance, opening and closing of cones and humidity sensors.<sup>[71,72]</sup> Here, we further progress the idea by combining vertically-aligned forests of CNTs (VACNTs) with PNIPAM. Combining the thermal response of PNIPAM with the high emissivity of CNT forests means that radiative heat can be transferred efficiently to the actuators to drive PNIPAM actuation. The CNTs bestow anisotropic properties to the composite material, both on the nanoscale (through vertical alignment of CNTs within the forests) and on the microscale. The overall microscale design of the CNT structure controls the type of motion observed during hydrogel actuation, allowing complex reversible motions to be achieved, such as anisotropic actuation on both the nanoscale and microscale.

The proof-of-concept actuators shown here demonstrate shape changes of various lattices, switching between high- and low-transparency states, and buckling. Further, this work provides an understanding of the actuation mechanisms, and we anticipate that the proposed composite microactuators ( $\mu$ actuators) have potential applications in color- and reflectivity-changing surfaces, thermoregulation, valves, pumps, and other flow-control devices.

## 2. Results and Discussion

### 2.1. Actuator Design and Fabrication

VACNT forests are grown using chemical vapor deposition from lithographically defined patterns on Si-wafers (Figure 1a). This method allows for the straightforward fabrication of any geometry in the form of a 2D vertical extrusion, with heights ranging from microns to millimeters.<sup>[73–75]</sup> The resulting structures have vertical mechanical properties determined by the covalent bonding along the length of the CNTs, combined with different lateral mechanical properties set by the interaction between neighboring CNTs.<sup>[76–78]</sup> A temperature-responsive hydrogel is formed via free-radical polymerization of *N*-isopropylacrylamide (NIPAM) using a redox initiator in the presence of a crosslinking agent, *N,N'*-methylene-bis-acrylamide (BIS). The resulting hydrogel is in a swollen state below  $T_c$ , and reversibly shrinks when the hydrogel is heated above  $T_c$  (Figure 1a).

When PNIPAM hydrogel is formed in situ on the CNT structures, the forests act as a scaffold to define its size and shape. Isotropic expansion and contraction of the hydrogel produces an anisotropic response in the CNT/PNIPAM composite due to the vertical nanoscale alignment of the CNTs: the induced strain of the composite is negligible vertically ( $\approx 1\%$ ), but significant laterally ( $\approx 60\%$ ) (Figure 1b; Figure S1, Supporting Information). The CNT forests resist strain along their growth axis due to the strength of the individual CNTs along their length, but the forests allow strain laterally as the nanotubes can move relative to each other within the forest.<sup>[78]</sup> Microscale anisotropy is achieved by growing CNTs in specific patterns instead of uniformly across a substrate. These patterned CNT forests act as a skeleton, about which bulk PNIPAM is formed to pull like a muscle, resulting in more complex motion on switching through  $T_c$  (Figure 1a). Both free and surface-bound actuators can be used, which demonstrate different behaviors (Figure 1c). Here, the microactuators ( $\mu$ actuators) are typically on the scale of hundreds of microns for ease of handling and imaging, but it is straightforward to scale them down to microns using the same fabrication procedure.

The actuators are fabricated by first growing the CNT forests in a desired pattern on a substrate (Figure 2a–c). A PNIPAM hydrogel precursor solution including initiator is then deposited onto the substrate, physisorbs onto the CNTs, and is polymerized in situ (taking care to ensure oxygen-free conditions, see Experimental Section) so that the CNTs are physically embedded in the gel (Figure 2d,e). The precursor solution selectively wets the CNTs by wicking into the nanostructures (improved by UV-ozone treatment, see Experimental Section), resulting in individual CNT/PNIPAM hydrogel composite structures with only a thin layer of hydrogel over the bare substrate (Figure S2a, Supporting Information). Depositing instead an excess of precursor solution creates a hydrogel layer with uniform thickness over the whole substrate, resulting in a bulk hydrogel film with CNT structures embedded throughout (Figure S2b, Supporting Information). The former method is ideal for actuators that are to be kept bound to the substrate, and the latter for actuators that are to be removed from the substrate – the bulk hydrogel films can be easily peeled away from the substrate (Figure 2g). This provides additional functionality since different behaviors are found when the actuator structures are surface-bound or free.

### 2.2. Behavior of Free CNT/PNIPAM Hydrogel $\mu$ actuators

A range of free actuator designs are tested, each demonstrating specific actuation behaviors (Figure 3). When multiple CNT/PNIPAM walls (Figure 3a) are embedded in a bulk hydrogel film, the separation of the structures decreases upon heating as the bulk hydrogel contracts more than the CNT/PNIPAM structures (Figure 3f). Honeycomb patterned CNT structures (Figure 3b) show strong optical absorptivity changes, as the CNT/PNIPAM skeleton contracts less than the bulk PNIPAM (Figure 3g) tilting the black sidewalls into full opacity (compounded by the increased turbidity of the hot PNIPAM). CNT forests can also be grown into structured sheets that have anisotropic mechanical properties emerging from the morphology

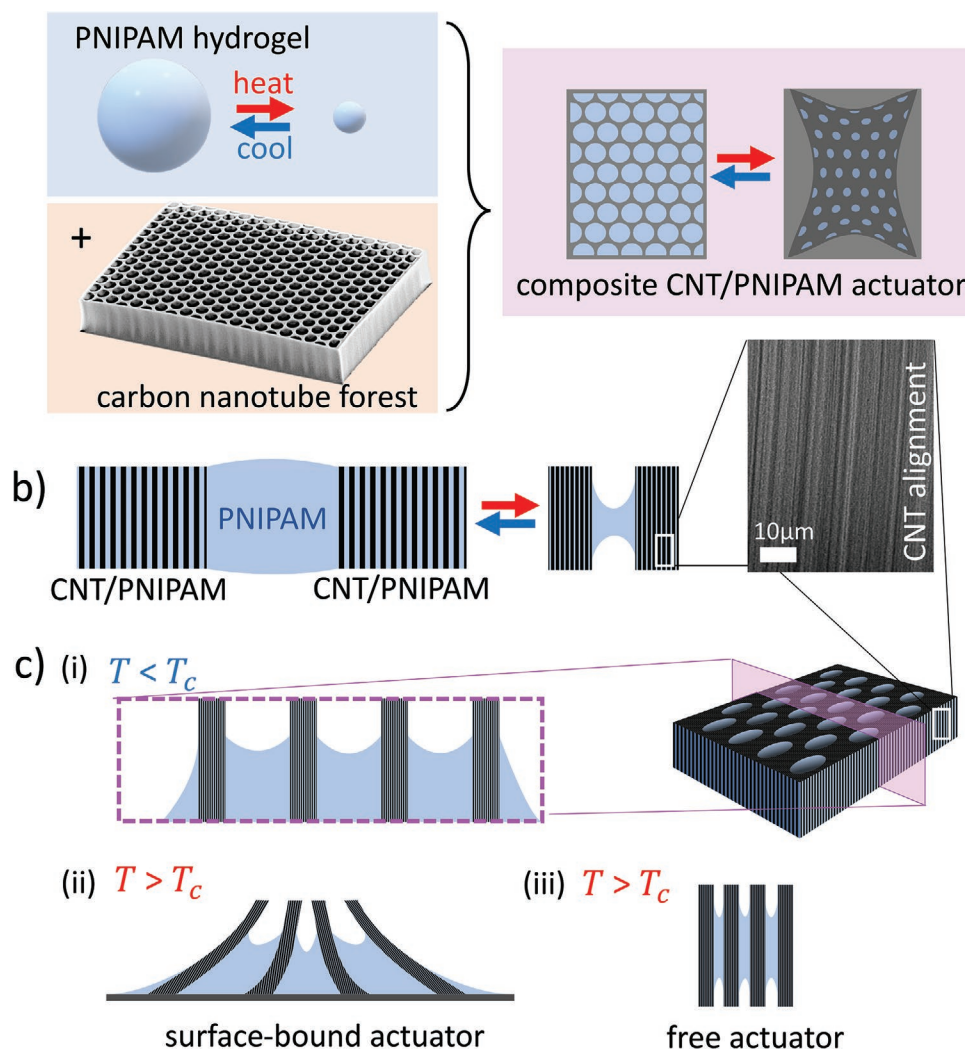


**Figure 1.** a) Schematic temperature response of PNIPAM and CNTs separately, and combined into exemplar CNT/PNIPAM composite structure. b) Schematic showing deformation of bulk PNIPAM and CNT/PNIPAM composite walls during actuation, demonstrating the anisotropic response that results from the vertical alignment of the CNTs. c) Schematic showing the morphology of an exemplar CNT/PNIPAM actuator (i) below  $T_c$  of PNIPAM, (ii) above  $T_c$  while surface-bound, and (iii) above  $T_c$  while free.

of their lattice (Figure 3c–e).<sup>[79]</sup> These, when formed into structured CNT/PNIPAM hydrogel composite sheets, show both macroscopic size changes (Figure 3h) and reversible changes in the shape of the lattice unit cell (Figure 3i,j). This shows the huge range of design freedoms available, accessing symmetry breaking and local buckling rotations in the unit cell (Figure 3i,j, white arrows), auxetic systems (Figure 3e), and offering opportunities for coupling the optical and mechanical response.

### 2.3. Behavior of Surface-Bound CNT/PNIPAM Hydrogel Actuators

Surface-bound actuators can show more complex actuation behaviors, as the surface binding boundary condition restricts the swelling and contraction of the PNIPAM (Figure 4; Movie S1, Supporting Information). Although the free actuators

show strong reflectance changes, their application is perhaps limited because the overall size of the structures also changes. By contrast, a surface-bound honeycomb actuator (Figure 4a,b) shows reflectance changes without any overall change in the structure area. The CNTs at the base of the structure bound to the substrate maintain the overall size, while the CNTs at the top of the structure far from the base become tilted by the contracting PNIPAM top surface, which pulls the CNT walls inwards. Viewed from the top, the cavities in the CNT structure thus close, absorbing incident light. This is supported by finite element simulations of the structure (Figure 4c,d). Reversible buckling behavior is also observed in surface-bound structures, as the differential expansion of the CNT/PNIPAM walls and the bulk PNIPAM in the cells is relieved by first-order buckling of the walls (Figure 4f). This matches accounts of corresponding structures in literature, which suggest that more complex buckling behaviors, including chiral actuation, can be achieved from similar structures via optimizing their geometry.<sup>[80,81]</sup>

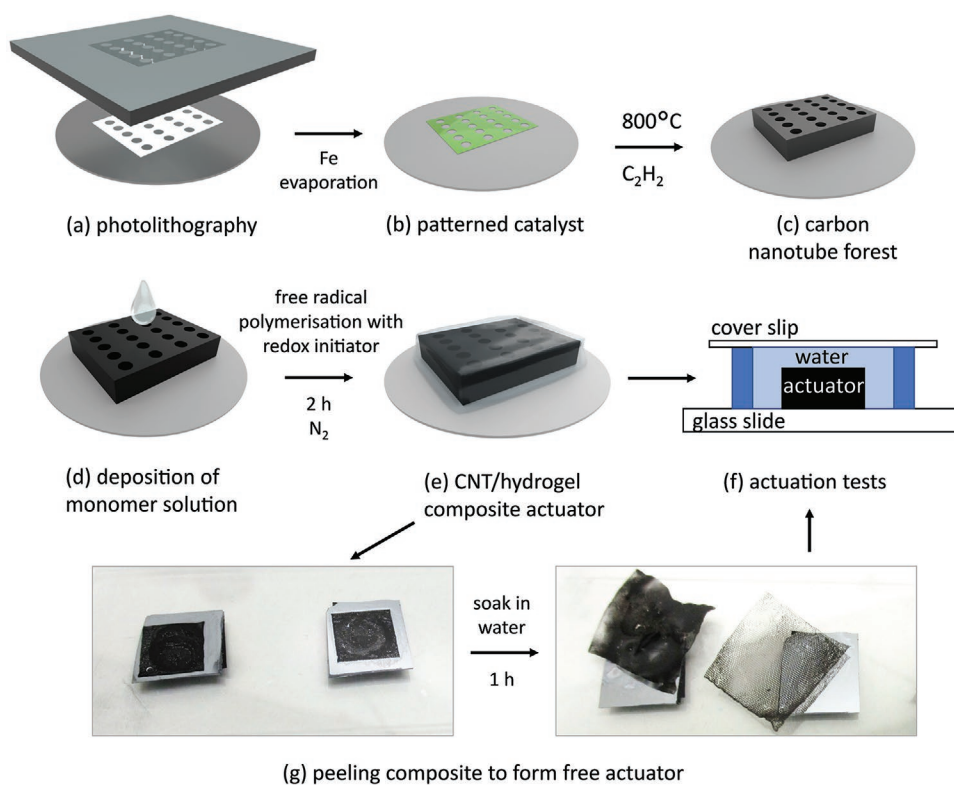


**Figure 2.** Schematic of fabrication and testing of CNT/PNIPAM hydrogel composite  $\mu$ actuators. Schematic shows a,b) patterning of CNT growth catalyst by photolithography, c) growth of CNTs by chemical vapor deposition, d,e) deposition and in situ polymerization of PNIPAM hydrogel on CNT microstructures, and f) setup used for testing the temperature response of the  $\mu$ actuators. g) Photographs of CNT/PNIPAM hydrogel actuators, with higher (left) and lower (right) density CNT lattice designs as skeletons, peeling from substrate when swelled in water.

## 2.4. Light Response of CNT/PNIPAM Hydrogel $\mu$ actuators

The composite actuators fabricated here are typically sub-millimeter, set by the initial CNT microstructure. This small size allows for faster response times, as the distance over which water must travel is reduced.<sup>[82]</sup> The use of CNTs also improves the response time, as they act as fluidic channels and so enhance water transport.<sup>[21,71,83,84]</sup> However, another factor contributing to the response time is heat transport through the structure and its surroundings. When inducing temperature changes using a hot plate, the response time is limited by heat conduction and convection (although the small size of the actuator again helps because there is less mass to heat). Switching times of less than 5 min are achieved using a hot plate, however much faster response times can be achieved by using optical heating.

The highly efficient optical absorption of CNTs is used here to create light-responsive actuators (Figure 5). Large area 532 nm laser illumination at  $\approx 20 \text{ W cm}^{-2}$  successfully induces contraction in the CNT/PNIPAM composite actuators (Movie S2, Supporting Information). This requires the presence of CNTs, as actuation is not observed in bulk PNIPAM using the same incident power (Figure S4, Supporting Information). The response time of the structure for optical driving is now on the scale of seconds instead of minutes (Figure 5a; Figure S5, Supporting Information). Local heating at the center of the laser spot is seen within 70 ms, as identified by the rapid

increase in opacity of PNIPAM in its hot state (dark region). The whole structure exceeds  $T_c$  after 1.3 s and is fully contracted less than 3 s after laser illumination begins. The contraction time here remains limited by heat transfer, as is clear from the difference in switching times between the center of the laser spot and the edges. The water transport limited response time of the actuator could be sped-up by optimizing the CNT structure design and the laser heating configuration. The return to the original shape of the structure takes 1–2 min, as there is so far no active cooling of the system, which would provide further speed-up.

Using a focused laser allows controlled local actuation (Figure 5b; Movie S3, Supporting Information). By lowering the laser power, there is insufficient photothermal input to heat the whole actuator above  $T_c$ , and thus only the center of the illuminated area actuates. This enables reversible highly-controlled changes in actuator morphology which are not simply predetermined by the shape of the actuator but can be adapted during use as needed. This, for instance, would enable hinging on the left or right side of an articulated device (Figure S6, Supporting Information). Note that the visible “hot spot” of laser heating is not necessarily centered around the laser focus spot (Figure 5b), due to the balance between heat absorption and heat loss. The edge of the shadow circle is the boundary at which the equilibrium of photothermal heating, heat transfer within the actuator, and heat loss to the environment result in a temperature below the  $T_c$  of PNIPAM (32 °C). The laser spot size is  $\approx 1 \text{ mm}^2$  across,

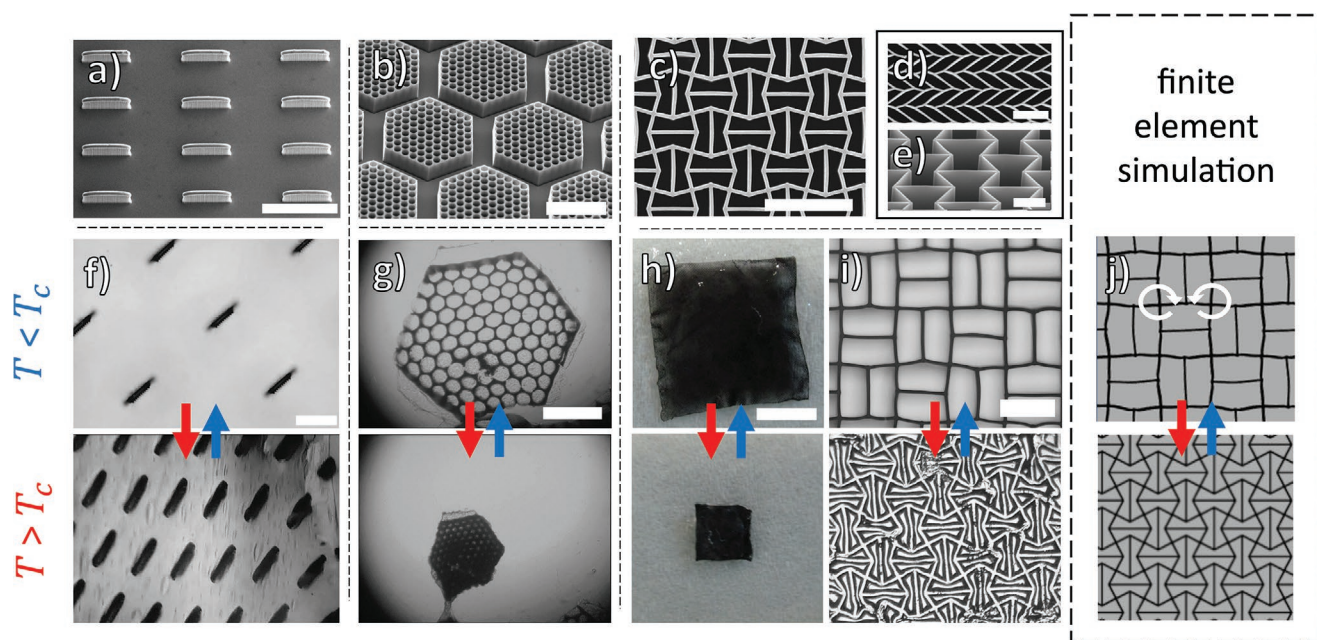


**Figure 3.** Scanning electron microscopy images (top row) of bare carbon nanotube structures used for  $\mu$ actuators fabrication, where (a,b,e) and are taken with the sample mounted at  $45^\circ$  to the electron beam, and (c,d) are taken with the electron beam normal to the sample surface. Reversible actuation (lower rows) of free CNT/PNIPAM composite hydrogel  $\mu$ actuators, demonstrating behaviors: f) change in density of CNT/PNIPAM microstructures embedded in bulk PNIPAM film, g) transparency change, h) macroscale size change, and i) microscale change in shape of lattice unit cell of CNT/hydrogel lattice with structure as in (c). j) Actuation behavior of lattice shown in (c,g) using finite element simulation, showing shape change via local rotations (white arrows). Scale bars are  $300\ \mu\text{m}$ ,  $300\ \mu\text{m}$ ,  $150\ \mu\text{m}$ ,  $100\ \mu\text{m}$ ,  $100\ \mu\text{m}$ ,  $200\ \mu\text{m}$ ,  $300\ \mu\text{m}$ ,  $5\ \text{mm}$ , and  $100\ \mu\text{m}$  in (a,b,c,d,e,f,g,h,i) respectively.

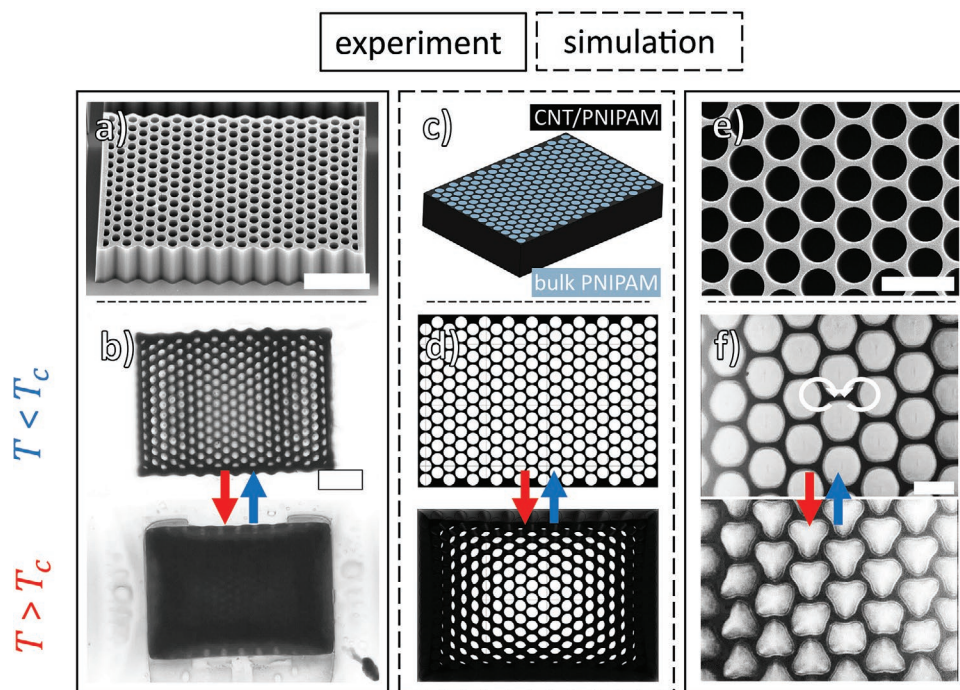


**Figure 4.** a) Scanning electron microscopy image of pristine carbon nanotube structure used for  $\mu$ actuator. b) Reversible actuation of surface-bound CNT/PNIPAM composite hydrogel  $\mu$ actuators, demonstrating transparency switch from opening and closing of inner cells. c) Schematic structure used for finite element simulation of CNT/PNIPAM hydrogel actuators showing d) contraction under deswelling that matches (b). e,f) As (a,b) but with higher magnification, showing shape changes of lattice unit cell by reversible buckling (f) and local rotations (white arrows). Scale bars are  $200\ \mu\text{m}$ ,  $200\ \mu\text{m}$ ,  $80\ \mu\text{m}$ , and  $40\ \mu\text{m}$  in (a,b,e,f) respectively.

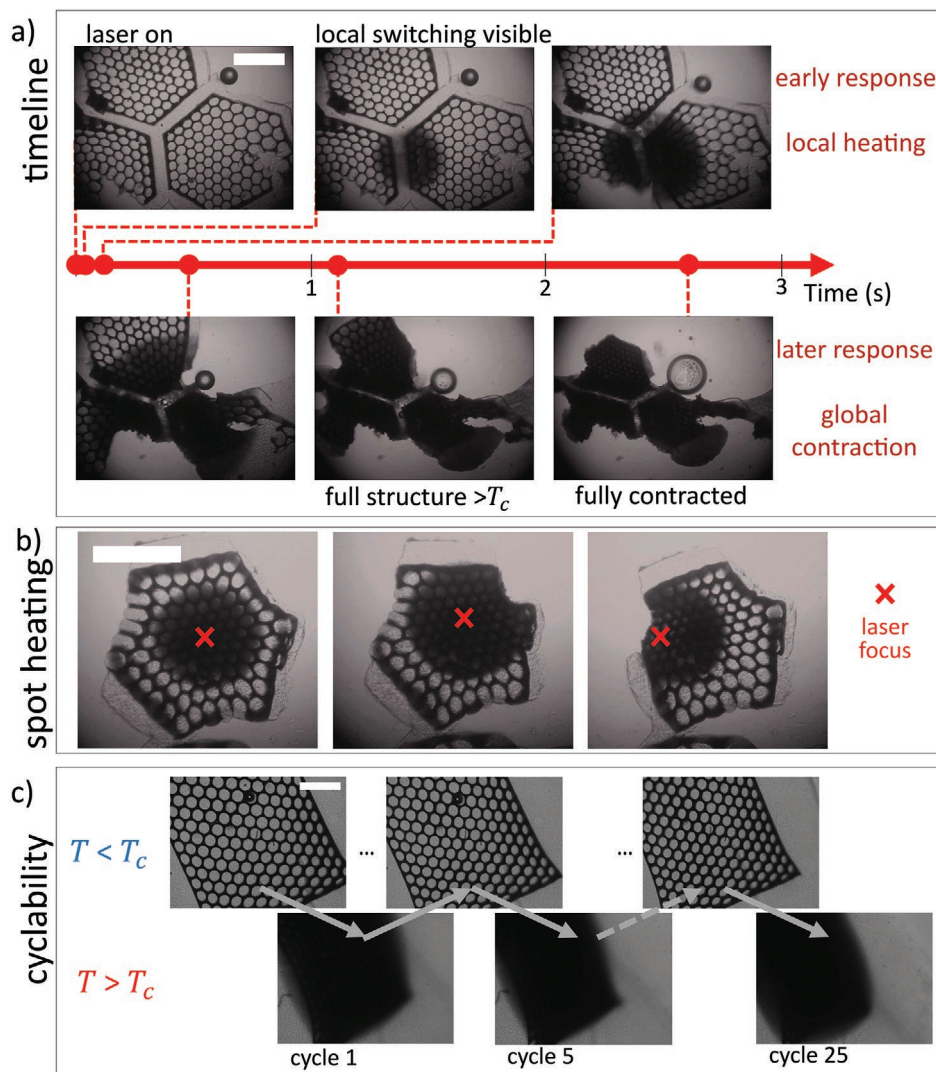


**Figure 5.** Light-responsive behavior of CNT/PNIPAM  $\mu$ actuators. a) Timeline with optical transmission images showing response of  $\mu$ actuator to illumination with 185 mW focused laser at 532 nm, showing local heating is observed within 70 ms of illumination and that the  $\mu$ actuator is fully contracted within 3 s. b) Optical microscopy images showing controlled local switching of a CNT/PNIPAM  $\mu$ actuator using 20 mW 532 nm laser. c) Images showing the cyclability of a CNT/PNIPAM  $\mu$ actuator, demonstrating that a large reversible switch in volume is consistent over at least 25 cycles. Scale bars are 300  $\mu$ m throughout.

with highest intensity at the point marked. When the laser spot is centered over the middle of the actuator, this results in a circle centered at the laser spot. However, when the laser spot is centered at the edge, the only significant photothermal heating is where the light is incident on CNTs, so heat is only generated within the actuator and thus the “hot spot” center is shifted away from the laser focus.

The shorter response times with light actuation make cyclability tests of such structures feasible. Over 25 cycles, actuators still show large reversible actuation (Figure 5c). Small changes in appearance likely arise from the actuator slightly moving during cycling. The actuation response still survives over this time (and likely indefinitely) as PNIPAM is known to maintain its actuation over >1000 cycles.<sup>[20,85]</sup> The limiting factor currently appears to be the CNT skeletal structure, as some structures show cracking in the CNT/PNIPAM walls after repeated

actuation (Figure S7, Supporting Information). This would only affect particularly severe actuation behaviors such as buckling, while others, such as transparency changes, would survive as they do not depend on contiguous CNT/PNIPAM structures.

### 3. Conclusion

Hydrogels are promising materials for the fabrication of soft actuators, but are limited by response time and their simple isotropic volume change. The composite carbon nanotube/poly(*N*-isopropylacrylamide) (CNT/PNIPAM) actuators in this paper address these challenges and bring hydrogel actuators closer to implementation. CNTs add direction-dependent properties to the hydrogel, and the resulting structures demonstrate anisotropic behavior on both the nanoscale and the microscale.

This fabrication process allows for actuators with a wide range of programmed movements. Behaviors such as opening and closing holes, transparency changes, and shape changes of each lattice unit cell are successfully demonstrated, with many more behaviors achievable in the future using diverse CNT structure designs. The small size of the structures contributes to a fast actuation time, with these CNT/PNIPAM hydrogel actuators reaching their fully contracted state in under 3 s globally, and under 70 ms locally. This time could be further decreased by optimizing the CNT skeleton design, decreasing the actuator size further, and enhancing the heating mechanism (since heating tests indicate that local actuator heating occurs in tens of microseconds). The addition of CNTs to PNIPAM hydrogels results in actuators that are both light- and heat-responsive, as CNTs have broadband strong absorption of optical and IR radiation. This allows for faster switching times, as the actuator can be directly radiatively heated rather than requiring the whole environment to be heated. The use of a laser beam for heating also demonstrated that switching can be locally controlled within a single actuator structure. This removes the restriction of an actuation response that is pre-determined only by the fabrication and initial design, giving responses that can be controlled at will post-fabrication.

#### 4. Experimental Section

*Patterned Growth of Vertically Aligned Carbon Nanotube Forests by Chemical Vapor Deposition:* CNT microstructures are grown on silicon and fused silica wafers with a catalyst layer of 9 nm Al<sub>2</sub>O<sub>3</sub> and 1 nm Fe. The catalyst pattern is defined by photolithography using AZ5214E photoresist, and the catalyst materials are deposited using e-beam evaporation. The CNT forest is grown for 1–2 min in a horizontal tube furnace at atmospheric pressure using gas flows 100/400/100 C<sub>2</sub>H<sub>4</sub>/H<sub>2</sub>/He. The samples are cooled by pulling the tube out of the heated length of the furnace while maintaining a growth atmosphere in order to improve the adhesion of the CNTs to the substrate.

*Redox Polymerization and Crosslinking of N-isopropylacrylamide:* N-isopropylacrylamide (NIPAM) (255 mg) and N,N'-methylenebis(acrylamide) (BIS) (2.25 mg) were added to 1.5 mL of water. Nitrogen gas was bubbled through this monomer solution for at least 15 min to remove oxygen. Potassium persulfate (KPS) solution (85 μL of 60 mg mL<sup>-1</sup> solution) and tetraethylenediamine (TEMED) (2.3 μL) were used as the initiator and accelerator respectively. A fresh KPS solution is made on the day to avoid degradation. UV-ozone treatment was used to hydrophilize the surface of the CNT sample to improve the wetting of the pre-polymer solution onto the CNT structures. After adding the KPS and TEMED, the pre-polymer solution was swirled to make a homogeneous solution and deposited onto the treated CNT sample within 10 min. The solution was deposited either by drop casting or spin coating at 1000 rpm for 30 s. The samples were kept under nitrogen for at least 2 h for the polymerization reaction to complete.

*Removing Composite Material from Substrate to Obtain Free Actuators:* When the actuators are to be removed from the substrate, the pre-polymer solution is deposited onto the sample thickly (i.e., at or greater than the CNT height) such that the whole surface is covered in a uniform film of hydrogel. Once polymerization has been completed, the sample is left in water overnight to fully hydrate. The thick, uniform layer of hydrogel expands upon hydration such that the sample peels itself away from the substrate to relieve the stress of the difference in size between the hydrogel film and the substrate.

*Actuation with Heated Stage:* The actuator to be tested is held in a dedicated chamber of water, which is placed on a Peltier component on a microscope stage. A thermocouple is placed in the chamber to

monitor the temperature. The sample is imaged while heating and cooling the chamber using the Peltier stage.

*Light Actuation:* The actuator is held in a chamber of water, which is placed on an optical microscope stage suitable for transmission imaging. A 532 nm laser is directed into the sample from below the stage, using a dichroic to reflect the laser upwards while still allowing the illumination white light to pass through for transmission imaging. A long-pass filter is placed before the microscope camera to block the laser beam, improving imaging and preventing damage to the camera. The incident optical power of the laser is varied from 15 to 185 mW.

#### Supporting Information

Supporting Information is available from the Wiley Online Library or from the author.

#### Acknowledgements

The authors acknowledge support from European Research Council (ERC) under Horizon 2020 research and innovation programme PICOFORCE (grant agreement no. 883703) and POSEIDON (grant agreement no. 861950), and ERC Consolidator Grant MIGHTY (8866005). The authors acknowledge funding from the EPSRC (EP/N016920/1, Cambridge NanoDTC EP/L015978/1, EP/L027151/1, EP/S022953/1, EP/P029426/1, EP/R020965/1, and 2338185).

#### Conflict of Interest

The authors declare no conflict of interest.

#### Data Availability Statement

Source data are provided with this paper and can be accessed at: <https://doi.org/10.17863/CAM.82776>.

#### Keywords

carbon nanotubes, hydrogel, light actuation, microactuators, soft robotics, vertically aligned CNTs

Received: January 25, 2022

Revised: March 21, 2022

Published online:

- [1] L. W. Xia, R. Xie, X. J. Ju, W. Wang, Q. Chen, L. Y. Chu, *Nat. Commun.* **2013**, *4*, 2226.
- [2] Y. Zhao, M. Hua, Y. Yan, S. Wu, Y. Alsaïd, X. He, *Annu. Rev. Control Robot. Auton. Syst.* **2022**, *5*, <https://doi.org/10.1146/annurev-control-042920>.
- [3] N. N. Ferreira, L. M. B. Ferreira, V. M. O. Cardoso, F. I. Boni, A. L. R. Souza, M. P. D. Gremião, *Eur. Polym. J.* **2018**, *99*, 117.
- [4] H. G. Schild, *Prog. Polym. Sci.* **1992**, *17*, 163.
- [5] L. Ionov, *Mater. Today* **2014**, *17*, 494.
- [6] S. J. Jeon, A. W. Hauser, R. C. Hayward, *Acc. Chem. Res.* **2017**, *50*, 161.
- [7] Y. Yang, Y. Tan, X. Wang, W. An, S. Xu, W. Liao, Y. Wang, *ACS Appl. Mater. Interfaces* **2018**, *10*, 7688.

- [8] X. Peng, T. Liu, C. Jiao, Y. Wu, N. Chen, H. Wang, *J. Mater. Chem. B* **2017**, *5*, 7997.
- [9] K. Shi, Z. Liu, Y. Y. Wei, W. Wang, X. J. Ju, R. Xie, L. Y. Chu, *ACS Appl. Mater. Interfaces* **2015**, *7*, 27289.
- [10] C. Ma, X. Le, X. Tang, J. He, P. Xiao, J. Zheng, H. Xiao, W. Lu, J. Zhang, Y. Huang, T. Chen, *Adv. Funct. Mater.* **2016**, *26*, 8670.
- [11] X. Qian, Y. Zhao, Y. Alsaïd, X. Wang, M. Hua, T. Galy, H. Gopalakrishna, Y. Yang, J. Cui, N. Liu, M. Marszewski, L. Pilon, H. Jiang, X. He, *Nat. Nanotechnol.* **2019**, *14*, 1048.
- [12] C. Ma, W. Lu, X. Yang, J. He, X. Le, L. Wang, J. Zhang, M. J. Serpe, Y. Huang, T. Chen, *Adv. Funct. Mater.* **2018**, *28*, 1704568.
- [13] H. W. Huang, M. S. Sakar, A. J. Petruska, S. Pané, B. J. Nelson, *Nat. Commun.* **2016**, *7*, 12263.
- [14] E. Lee, D. Kim, H. Kim, J. Yoon, *Sci. Rep.* **2015**, *5*, 15124.
- [15] S. Purushotham, R. V. Ramanujan, *Acta Biomater.* **2010**, *6*, 502.
- [16] J. Tang, Z. Tong, Y. Xia, M. Liu, Z. Lv, Y. Gao, T. Lu, S. Xie, Y. Pei, D. Fang, T. J. Wang, *J. Mater. Chem. B* **2018**, *6*, 2713.
- [17] T. Shen, M. G. Font, S. Jung, M. L. Gabriel, M. P. Stoykovich, F. J. Vernerey, *Sci. Rep.* **2017**, *7*, 16178.
- [18] H. Liu, Y. Zhang, S. Ma, Y. Alsaïd, X. Pei, M. Cai, X. He, F. Zhou, *Adv. Sci.* **2021**, *8*, 2102800.
- [19] C. Yao, Z. Liu, C. Yang, W. Wang, X. J. Ju, R. Xie, L. Y. Chu, *Adv. Funct. Mater.* **2015**, *25*, 2980.
- [20] T. Fujigaya, T. Morimoto, Y. Niidome, N. Nakashima, *Adv. Mater.* **2008**, *20*, 3610.
- [21] X. Zhang, C. L. Pint, M. H. Lee, B. E. Schubert, A. Jamshidi, K. Takei, H. Ko, A. Gillies, R. Bardhan, J. J. Urban, M. Wu, R. Fearing, A. Javey, *Nano Lett.* **2011**, *11*, 3239.
- [22] J. Kim, J. A. Hanna, M. Byun, C. D. Santangelo, R. C. Hayward, *Science* **2012**, *335*, 1201.
- [23] Z. L. Wu, M. Moshe, J. Greener, H. Therien-Aubin, Z. Nie, E. Sharon, E. Kumacheva, *Nat. Commun.* **2013**, *4*, 1586.
- [24] S. Fusco, M. S. Sakar, S. Kennedy, C. Peters, R. Bottani, F. Starsich, A. Mao, G. A. Sotiriou, S. Pané, S. E. Pratsinis, D. Mooney, B. J. Nelson, *Adv. Mater.* **2014**, *26*, 952.
- [25] Y. Zhou, A. W. Hauser, N. P. Bende, M. G. Kuzyk, R. C. Hayward, *Adv. Funct. Mater.* **2016**, *26*, 5447.
- [26] L. Liu, S. Jiang, Y. Sun, S. Agarwal, *Adv. Funct. Mater.* **2016**, *26*, 1021.
- [27] J. H. Na, A. A. Evans, J. Bae, M. C. Chiappelli, C. D. Santangelo, R. J. Lang, T. C. Hull, R. C. Hayward, *Adv. Mater.* **2015**, *27*, 79.
- [28] J. L. Silverberg, J. H. Na, A. A. Evans, B. Liu, T. C. Hull, C. D. Santangelo, R. J. Lang, R. C. Hayward, I. Cohen, *Nat. Mater.* **2015**, *14*, 389.
- [29] A. Sidorenko, T. Krupenkin, A. Taylor, P. Fratzl, J. Aizenberg, *Science* **2007**, *315*, 487.
- [30] Y. S. Kim, M. Liu, Y. Ishida, Y. Ebina, M. Osada, T. Sasaki, T. Hikima, M. Takata, T. Aida, *Nat. Mater.* **2015**, *14*, 1002.
- [31] Z. Sun, Y. Yamauchi, F. Araoka, Y. S. Kim, J. Bergueiro, Y. Ishida, Y. Ebina, T. Sasaki, T. Hikima, T. Aida, *Angew. Chem., Int. Ed.* **2018**, *57*, 15772.
- [32] A. Sidorenko, T. Krupenkin, J. Aizenberg, *J. Mater. Chem.* **2008**, *18*, 3841.
- [33] P. Kim, L. D. Zarzar, X. He, A. Grinthal, J. Aizenberg, *Curr. Opin. Solid State Mater. Sci.* **2011**, *15*, 236.
- [34] A. Sutton, T. Shirman, J. V. I. Timonen, G. T. England, P. Kim, M. Kolle, T. Ferrante, L. D. Zarzar, E. Strong, J. Aizenberg, *Nat. Commun.* **2017**, *8*, 14700.
- [35] M. R. Islam, M. J. Serpe, *RSC Adv.* **2014**, *4*, 31937.
- [36] G. Isapour, B. H. Miller, M. Kolle, *Adv. Photonics Res.* **2022**, *3*, 2100043.
- [37] M. R. Islam, S. Xie, D. Huang, K. Smyth, M. J. Serpe, *Anal. Chim. Acta* **2015**, *898*, 101.
- [38] A. Nishiguchi, H. Zhang, S. Schweizerhof, M. F. Schulte, A. Mourran, M. Möller, *ACS Appl. Mater. Interfaces* **2020**, *12*, 12176.
- [39] S. E. Bakarich, R. Gorkin, M. in het Panhuis, G. M. Spinks, *Macromol. Rapid Commun.* **2015**, *36*, 1211.
- [40] D. Han, Z. Lu, S. A. Chester, H. Lee, *Sci. Rep.* **2018**, *8*, 1963.
- [41] X. Peng, T. Liu, Q. Zhang, C. Shang, Q. W. Bai, H. Wang, *Adv. Funct. Mater.* **2017**, *27*, 1701962.
- [42] B. Peng, M. Locascio, P. Zapol, S. Li, S. L. Mielke, G. C. Schatz, H. D. Espinosa, *Nat. Nanotechnol.* **2008**, *3*, 626.
- [43] Y. Bai, H. Yue, J. Wang, B. Shen, S. Sun, S. Wang, H. Wang, X. Li, Z. Xu, R. Zhang, F. Wei, *Science* **2020**, *369*, 1104.
- [44] S. Ogata, Y. Shibutani, *Phys. Rev. B* **2003**, *68*, 165409.
- [45] M. R. Falvo, G. J. Clary, R. M. Taylor, V. Chi, F. P. Brooks, S. Washburn, R. Superfine, *Nature* **1997**, *389*, 582.
- [46] J. Suhr, P. Victor, L. Ci, S. Sreekala, X. Zhang, O. Nalamasu, P. M. Ajayan, *Nat. Nanotechnol.* **2007**, *2*, 417.
- [47] K. Mizuno, J. Ishii, H. Kishida, Y. Hayamizu, S. Yasuda, D. N. Futaba, M. Yumura, K. Hata, *Proc. Natl. Acad. Sci. USA* **2009**, *106*, 6044.
- [48] Z. P. Yang, L. Ci, J. A. Bur, S. Y. Lin, P. M. Ajayan, *Nano Lett.* **2008**, *8*, 446.
- [49] A. A. Adewunmi, S. Ismail, A. S. Sultan, *J. Inorg. Organomet. Polym. Mater.* **2016**, *26*, 717.
- [50] M. Mihajlovic, M. Mihajlovic, P. Y. W. Dankers, R. Masereeuw, R. P. Sijbesma, *Macromol. Biosci.* **2019**, *19*, 1800173.
- [51] L. Liu, A. H. Barber, S. Nuriel, H. D. Wagner, *Adv. Funct. Mater.* **2005**, *15*, 975.
- [52] H. U. Rehman, Y. Chen, Y. Guo, Q. Du, J. Zhou, Y. Guo, H. Duan, H. Li, H. Liu, *Composites, Part A* **2016**, *90*, 250.
- [53] K. Shah, D. Vasileva, A. Karadaghy, S. P. Zustiak, *J. Mater. Chem. B* **2015**, *3*, 7950.
- [54] W. Dong, C. Huang, Y. Wang, Y. Sun, P. Ma, M. Chen, *Int. J. Mol. Sci.* **2013**, *14*, 22380.
- [55] X. Liu, A. L. Miller, S. Park, B. E. Waletzki, A. Terzic, M. J. Yaszemski, L. Lu, *J. Mater. Chem. B* **2016**, *4*, 6930.
- [56] C. M. Homenick, H. Sheardown, A. Adronov, *J. Mater. Chem.* **2010**, *20*, 2887.
- [57] M. K. Bayazit, L. S. Clarke, K. S. Coleman, N. Clarke, *J. Am. Chem. Soc.* **2010**, *132*, 15814.
- [58] V. Saez-Martinez, A. Garcia-Gallastegui, C. Vera, B. Olalde, I. Madarieta, I. Obieta, N. Garagorri, *J. Appl. Polym. Sci.* **2011**, *120*, 124.
- [59] S. H. Hong, T. T. Tung, L. K. H. Trang, T. Y. Kim, K. S. Suh, *Colloid Polym. Sci.* **2010**, *288*, 1013.
- [60] S. Tamesue, S. Hasegawa, R. Ishizaki, K. Hashimoto, T. Mitsumata, N. Tsubokawa, T. Yamauchi, *Polym. J.* **2015**, *47*, 709.
- [61] T. Sun, H. Liu, W. Song, X. Wang, L. Jiang, L. Li, D. Zhu, *Angew. Chem., Int. Ed.* **2004**, *43*, 4663.
- [62] T. Shiraki, A. Dawn, T. N. L. Le, Y. Tsuchiya, S. I. Tamaru, S. Shinkai, *Chem. Commun.* **2011**, *47*, 7065.
- [63] C. Yin, F. Wei, S. Fu, Z. Zhai, Z. Ge, L. Yao, M. Jiang, M. Liu, *ACS Appl. Mater. Interfaces* **2021**, *13*, 47147.
- [64] Y. Yamamoto, K. Kanao, T. Arie, S. Akita, K. Takei, *ACS Appl. Mater. Interfaces* **2015**, *7*, 11002.
- [65] R. A. MacDonald, C. M. Vogge, M. Kariolis, J. P. Stegemann, *Acta Biomater.* **2008**, *4*, 1583.
- [66] S. R. Shin, C. Shin, A. Memic, S. Shadmehr, M. Miscuglio, H. Y. Jung, S. M. Jung, H. Bae, A. Khademhosseini, X. Tang, M. R. Dokmeci, *Adv. Funct. Mater.* **2015**, *25*, 4486.
- [67] M. De Volder, S. Park, S. Tawfick, A. J. Hart, *Nat. Commun.* **2014**, *5*, 4512.
- [68] M. F. L. De Volder, S. Tawfick, S. J. Park, A. J. Hart, *ACS Nano* **2011**, *5*, 7310.
- [69] R. M. Erb, J. S. Sander, R. Grisch, A. R. Studart, *Nat. Commun.* **2013**, *4*, 1712.
- [70] L. Hu, Y. Wan, Q. Zhang, M. J. Serpe, *Adv. Funct. Mater.* **2020**, *30*, 1903471.
- [71] M. de Volder, S. H. Tawfick, D. Copic, A. J. Hart, *Soft Matter* **2011**, *7*, 9844.

- [72] L. Ionov, *Adv. Funct. Mater.* **2013**, 23, 4555.
- [73] T. Sato, H. Sugime, S. Noda, *Carbon* **2018**, 136, 143.
- [74] H. Sugime, T. Sato, R. Nakagawa, C. Cepek, S. Noda, *ACS Nano* **2019**, 13, 13208.
- [75] M. De Volder, S. H. Tawfick, S. J. Park, D. Copic, Z. Zhao, W. Lu, A. J. Hart, *Adv. Mater.* **2010**, 22, 4384.
- [76] Y. Bai, R. Zhang, X. Ye, Z. Zhu, H. Xie, B. Shen, D. Cai, B. Liu, C. Zhang, Z. Jia, S. Zhang, X. Li, F. Wei, *Nat. Nanotechnol.* **2018**, 13, 589.
- [77] Y. Li, H. I. Kim, B. Wei, J. Kang, J. B. Choi, J. Do Nam, J. Suhr, *Nanoscale* **2015**, 7, 14299.
- [78] M. R. Maschmann, G. J. Ehlert, S. Tawfick, A. J. Hart, J. W. Baur, *Carbon* **2014**, 66, 377.
- [79] C. Schumacher, S. Marschner, M. Gross, B. Thomaszewski, *ACM Trans. Graph.* **2018**, 37, 15.
- [80] S. H. Kang, S. Shan, W. L. Noorduin, M. Khan, J. Aizenberg, K. Bertoldi, *Adv. Mater.* **2013**, 25, 3380.
- [81] S. Li, B. Deng, A. Grinthal, A. Schneider-Yamamura, J. Kang, R. S. Martens, C. T. Zhang, J. Li, S. Yu, K. Bertoldi, J. Aizenberg, *Nature* **2021**, 592, 386.
- [82] Y. Li, T. Tanaka, *J. Chem. Phys.* **1990**, 92, 1365.
- [83] S. Joseph, N. R. Aluru, *Nano Lett.* **2008**, 8, 452.
- [84] A. Kalra, S. Garde, G. Hummer, *Proc. Natl. Acad. Sci. USA* **2003**, 100, 10175.
- [85] T. Jiang, X. Zhao, X. Yin, R. Yang, G. Tan, *Appl. Energy* **2021**, 287, 116573.